Applied Catalysis B: Environmental 182 (2016) 456–468

Contents lists available at ScienceDirect

Applied Catalysis B: Environmental

journal homepage: www.elsevier.com/locate/apcatb

Visible light-assisted heterogeneous Fenton with $ZnFe_2O_4$ for the degradation of Orange II in water

Chun Cai [a,b], Zhuoyue Zhang [a], Jin Liu [a], Ni Shan [a], Hui Zhang [a,*], Dionysios D. Dionysiou [b,**]

[a] Department of Environmental Engineering, Wuhan University, Wuhan 430079, China
[b] Environmental Engineering and Science Program, University of Cincinnati, OH 45221-0012, United States

ARTICLE INFO

Article history:
Received 29 June 2015
Received in revised form 31 August 2015
Accepted 29 September 2015
Available online 9 October 2015

Keywords:
$ZnFe_2O_4$ nanoparticles
Visible-light irradiation
Hydroxyl radical
Photocatalysis
Fenton

ABSTRACT

In this study, a visible (Vis) light response photocatalyst was synthesized via a simple reduction–oxidation method. The structure, morphology and optical properties of the catalyst were well characterized. The absorption capability of $ZnFe_2O_4$ in visible-light region was demonstrated by the high rate of Orange II decolorization under Vis/$ZnFe_2O_4$/H_2O_2 process. Guided by studies to explore the effects of radical scavengers and to quantify the yield of hydroxyl radical (•OH) production, •OH on the surface of the catalyst was found to be the dominating reactive species for the Orange II removal. Moreover, $ZnFe_2O_4$ maintained high activity, crystallinity and extremely low iron and zinc leaching during repeated experiments. The intermediate products were identified by GC–MS and a possible pathway is accordingly proposed to elucidate the mechanism of Orange II degradation by •OH. In addition, high extent of mineralization was obtained as the chemical oxygen demand (COD) and total organic carbon (TOC) removal efficiencies were 86.6% and 60.4%, respectively, within 60 min reaction. The toxicity tests with activated sludge indicated that the toxicity of the solution increased during the first 30 min but then decreased significantly as the oxidation proceeded.

1. Introduction

Recently, the increasing use of dyes in numerous industries has led to a rise in the disposal of large amounts of dye wastewater [1,2]. Among these dyes, up to 70% are azo compounds [3,4]. Orange II ($C_{16}H_{11}N_2NaO_4S$), also called Acid Orange 7, is an anionic azo dye widely employed in various industries, including paper, printing, food, cosmetics, textile and leather [5,6]. Generally, Orange II presents good resistance to UV or solar light irradiation and microbial attack and sometimes may produce more hazardous intermediates during the degradation process [7]. Therefore, research on the development of effective and practical treatment processes for removal of Orange II has attracted increasing interest in recent years.

Nowadays, advanced oxidation processes (AOPs) based on the generation of highly reactive hydroxyl radicals (•OH, $E^0 = 2.80$ V/SHE) are commonly recognized as potential alternative technologies for the degradation of recalcitrant contaminants [8]. Among AOPs, the Fenton process is simple, inexpensive, and easy to run under mild conditions of temperature and pressure [3]. During the Fenton reaction, hydrogen peroxide (H_2O_2) is activated by Fe^{2+} under acidic solution (pH 3) to generate •OH (Eq. (1)) [6]. However, the recovery of Fe^{2+} through Eq. (2) is extremely slow [9]. Thus, ultraviolet (UV) light or electrochemical technology is frequently employed to the Fenton system for the regeneration of Fe^{2+} [1,10,11]. In the presence of UV irradiation, Fe^{2+} can be recycled and more hydroxyl radicals can be formed through Eq. (3) [12].

$$H_2O_2 + Fe^{2+} \rightarrow Fe^{3+} + {}^{\bullet}OH + OH^- \quad (1)$$

$$Fe^{3+} + H_2O_2 \rightarrow Fe^{2+} + HO_2{}^- + H^+ \quad (2)$$

$$Fe(OH)^{2+} + h\nu \rightarrow Fe^{2+} + {}^{\bullet}OH \quad (3)$$

Unfortunately, it is well known that only 4–5% of solar energy belongs to UV light, while visible (Vis) light covers about 45% of the energy [13,14]. In addition, the major drawbacks of homogeneous photo-Fenton process, such as the tight range of pH and further treatment of iron sludge, would finally increase the overall cost for water treatment [15,16]. Therefore, exploring highly efficient and low cost Vis light responsive heterogeneous photocatalysts is currently considered as a hot research topic [14,17]. In recent years, many studies have been reported for the heterogeneous photochemical removal of organic dyes by Vis-light/catalyst/H_2O_2

* Corresponding author. Fax: +86 27 68778893.
** Corresponding author. Fax: +1 513 5564162.
E-mail addresses: eeng@whu.edu.cn (H. Zhang), dionysios.d.dionysiou@uc.edu, dionysdd@ucmail.uc.edu (D.D. Dionysiou).

http://dx.doi.org/10.1016/j.apcatb.2015.09.056
0926-3373/

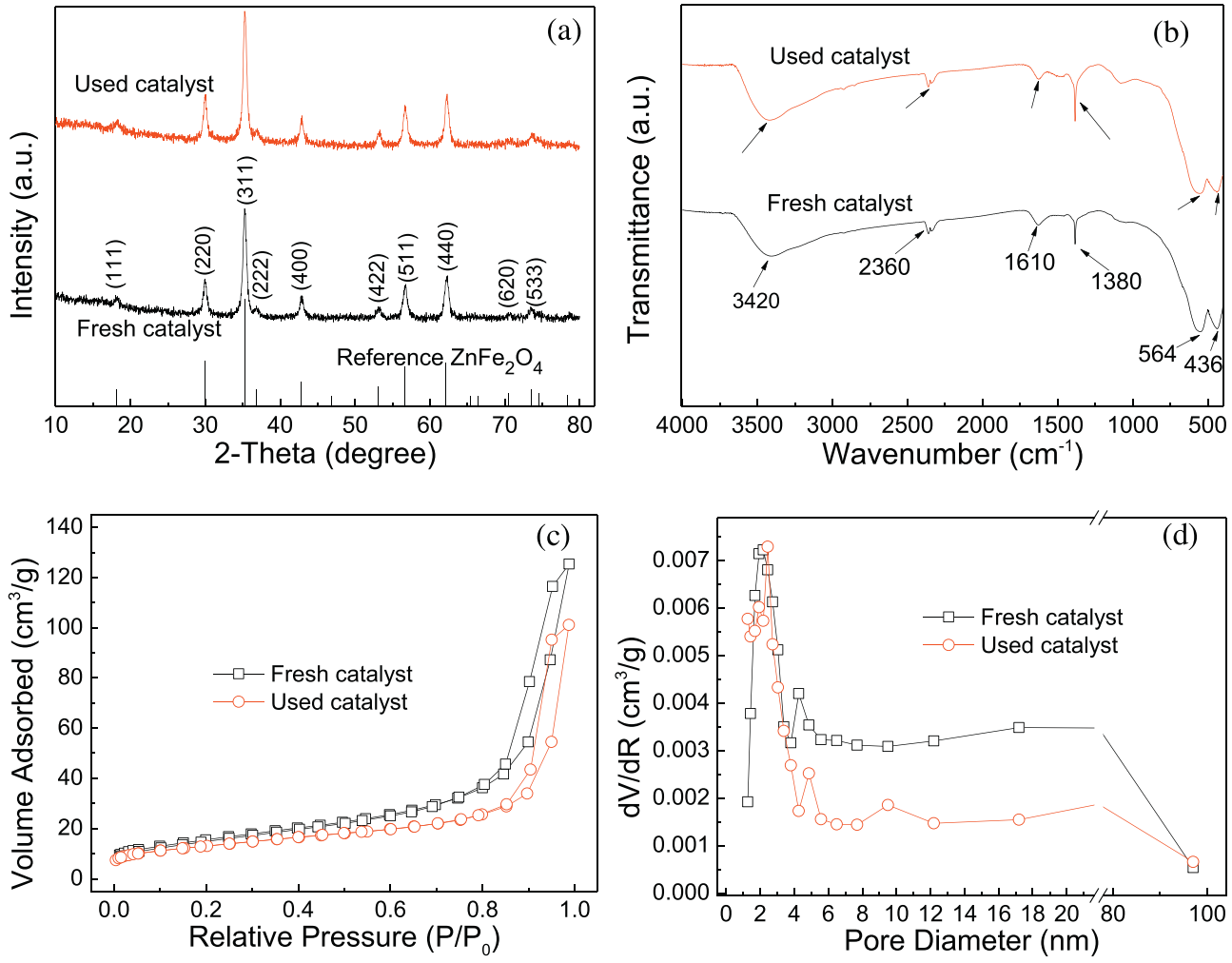

Fig. 1. (a) XRD patterns, (b) FTIR spectra, (c) nitrogen adsorption–desorption isotherm curves, (d) BJH pore size distribution curves of the $ZnFe_2O_4$.

process [18–21], and the decomposition rate of H_2O_2 is considered as one of the crucial factors on the photocatataytic degradation efficiency [13]. Thus, the development of photocatalysts with enhanced Vis-light-driven activity is of high interest.

Among various materials applied as photocatalysts with sunlight, the spinel ferrites are proposed as potential catalysts because of their narrow band gap and high stability [14]. Particularly, zinc ferrite ($ZnFe_2O_4$), which is non-expensive with a relatively narrow band gap of 1.9 eV, has drawn widespread attention in photocatalytic treatment of contaminants [22]. Additionally, $ZnFe_2O_4$ could react with H_2O_2 to produce $^{\bullet}OH$ due to its intrinsic peroxidase-like activity [23]. Hence, it can be expected that $ZnFe_2O_4$ might show better performance under Vis-light/H_2O_2 process.

It was reported that the synthesis condition and process had great influence on the physical and chemical properties such as the size and structure of spinel ferrites [19]. Up to now, various synthesis methods have been applied for $ZnFe_2O_4$, such as co-precipitation, sol–gel, hydrothermal, solvothermal, thermal decomposition, microwave irradiation, and combustion methods [24,25]. Among these routes, hydrothermal synthesis has been considered as one of the effective and economic approaches due to its relative low cost, short process time, homogeneity, reproducibility, energy efficiency, environmental friendliness, and simplicity, compared to other conventional methods [26,27]. Besides, many heterogeneous catalysts suffer from leaching problems. The concentration of Fe ions is usually high due to a significant degree of leaching out from the heterogeneous catalysts during the photo-Fenton process [28]. Therefore, a relatively facile method for the fabrication of smaller and uniform $ZnFe_2O_4$ catalyst via reduction–oxidation route was improved in this study, which included easily achievable reduction at ambient atmosphere. Then, the iron nuclei were oxidized in a separate hydrothermal process [25,26].

Herein, in this study, the Vis-light-assisted catalyst $ZnFe_2O_4$ was synthesized by a novel reduction–oxidation method mentioned above and the catalyst was characterized by transmission electron microscope (TEM), X-ray diffraction (XRD), X-ray photoelectron spectroscopy (XPS) and scanning electron microscopy with an energy dispersive spectrometer (SEM–EDS) before and after reaction. The photocatalytic activity of $ZnFe_2O_4$ was investigated using Orange II as a target contaminant under Vis-light irradiation together with H_2O_2. The influence of important variables such as initial pH, catalyst dosage, H_2O_2 concentration and visible light power were investigated. A possible mechanism for degradation of Orange II in the Vis/$ZnFe_2O_4$/H_2O_2 process was elucidated. The intermediate products were determined by GC–MS and a possible degradation pathway of Orange II was suggested. The mineralization of Orange II in terms of total organic carbon (TOC) removal efficiency and chemical oxygen demand (COD) removal efficiency together with the variation of toxicity to activated sludge were also studied.

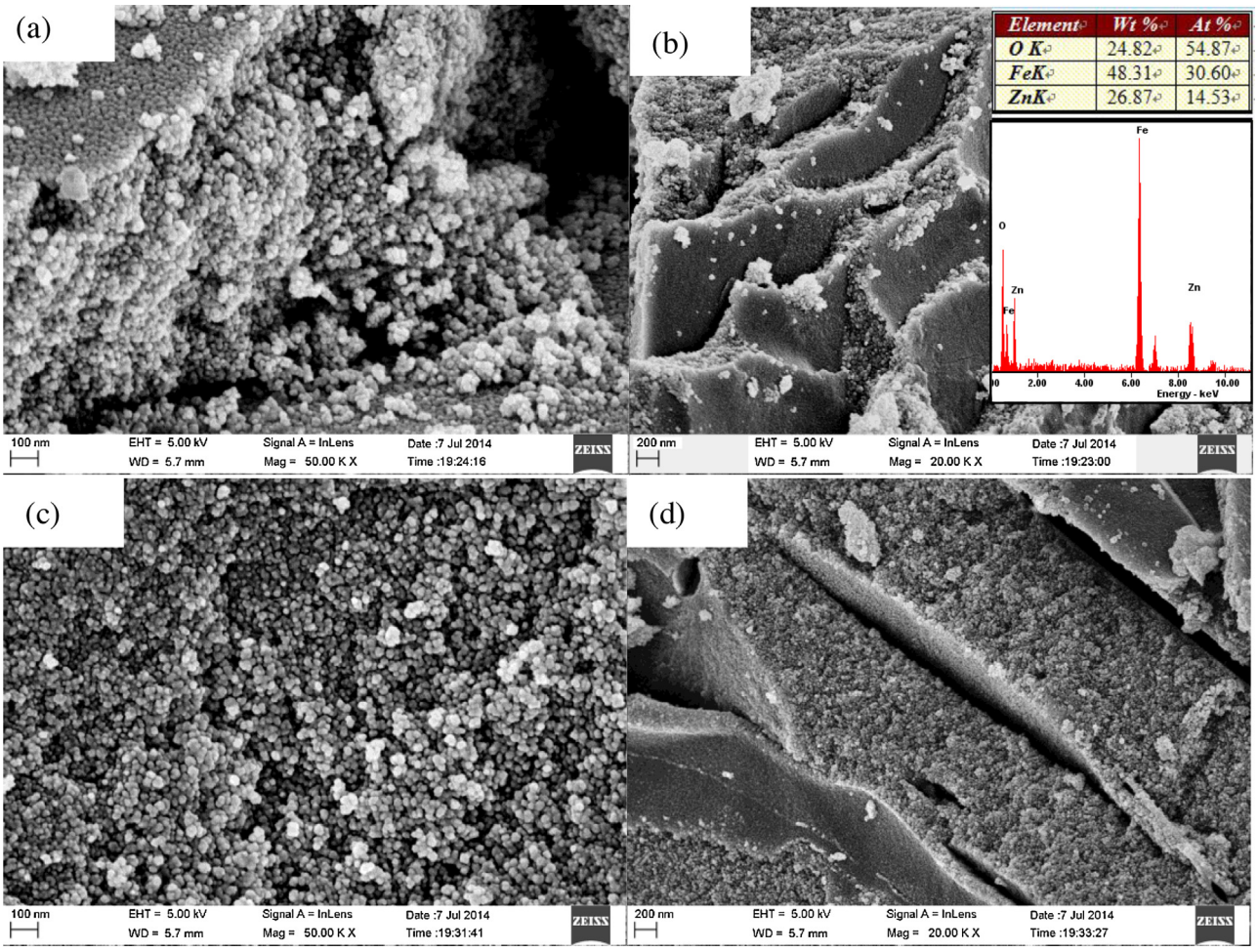

Fig. 2. FESEM micrographs of fresh (a and b), and used (c and d) $ZnFe_2O_4$ powders. Inset in this figure (b) shows the EDS results.

2. Experimental

2.1. Reagents and materials

The chemicals were used as purchased without further purification. Orange II ($C_{16}H_{11}N_2NaO_4S$) with reagent purity grade was purchased from Shanghai No. 3 Reagent Factory (China). Other reagents such as ferric nitrate ($Fe(NO_3)_3{\cdot}9H_2O$), zinc nitrate ($Zn(NO_3)_2{\cdot}6H_2O$) and sodium borohydride ($NaBH_4$) were of analytical grade and the solutions were prepared using deionized water (the specific conductivity was less than 5 μs/cm), which was obtained via a water purification system (Youpu Instrument Co., Xian, China).

2.2. Synthesis of $ZnFe_2O_4$ catalyst

The $ZnFe_2O_4$ catalyst was prepared according to the previously published approach [26,29]. Typically, two separate solutions were required before the synthesis. Solution I: $Fe(NO_3)_3{\cdot}9H_2O$ and $Zn(NO_3)_2{\cdot}6H_2O$ were dissolved in 50 mL of deionized water and the molar ratio of $[Fe^{3+}]$ and $[Zn^{2+}]$ was 2:1 ($[Fe^{3+}] = 0.2$ M). Solution II: $NaBH_4$ was prepared in 50 mL water deionized solution and the concentration of $NaBH_4$ was 0.4 M ($[Fe^{3+}]/[NaBH_4] = 1:2$). Then Solution II was rapidly added into the solution I within 30 min and mixed for 1 h under vigorous stirring. The mixture slurry was then maintained at 120 °C for 12 h in the Teflon-lined stainless autoclave. The autoclave was further cooled down to ambient temperature, and the obtained suspension was washed with deionized water for several times and then ethanol, separately. Finally, the solid samples were dried at 70 °C for one night.

2.3. Characterization

The properties of $ZnFe_2O_4$ samples were measured by Quantachrome NOVA2000e analyzer (USA) at 77 K and the results are provided in Table S1 (Supplementary data). The crystallographic structure and the mineralogy of the $ZnFe_2O_4$ catalysts were obtained on a PANalytical X'Pert Pro XRD system. Fourier transform infrared (FTIR) spectra were achieved on a Nicolet Nexus spectrometer. Microanalyses of the samples were recorded using a Field-Emission SEM (Zeiss SIGMA FESEM, Germany) equipped with an EDS analyzer (fixed probe) for the determination of iron and zinc (EDAX Genesis, USA). The morphology of the catalysts were determined by TEM (PhiliPMS CM120 microscope operated at 120 kV). XPS was detected on a ESCALAB 250Xi spectrometer (Thermo Fisher, USA) equipped with AlKα X-ray source. The scan UV–vis spectrophotometer (UV–vis DRS: UV-2450, Shimadzu, Japan) equipped with an integrating sphere assembly was employed to determine the UV–vis diffuse reflection spectra, and a baseline was recorded using barium sulfate.

2.4. Photocatalytic reaction

A schematic of the experiment setup is depicted (Fig. S1, Supplementary data). The visible light source was a xenon high intensity discharge lamp (X-HID) (Foshan Leimai Lighting Applicance Co.,

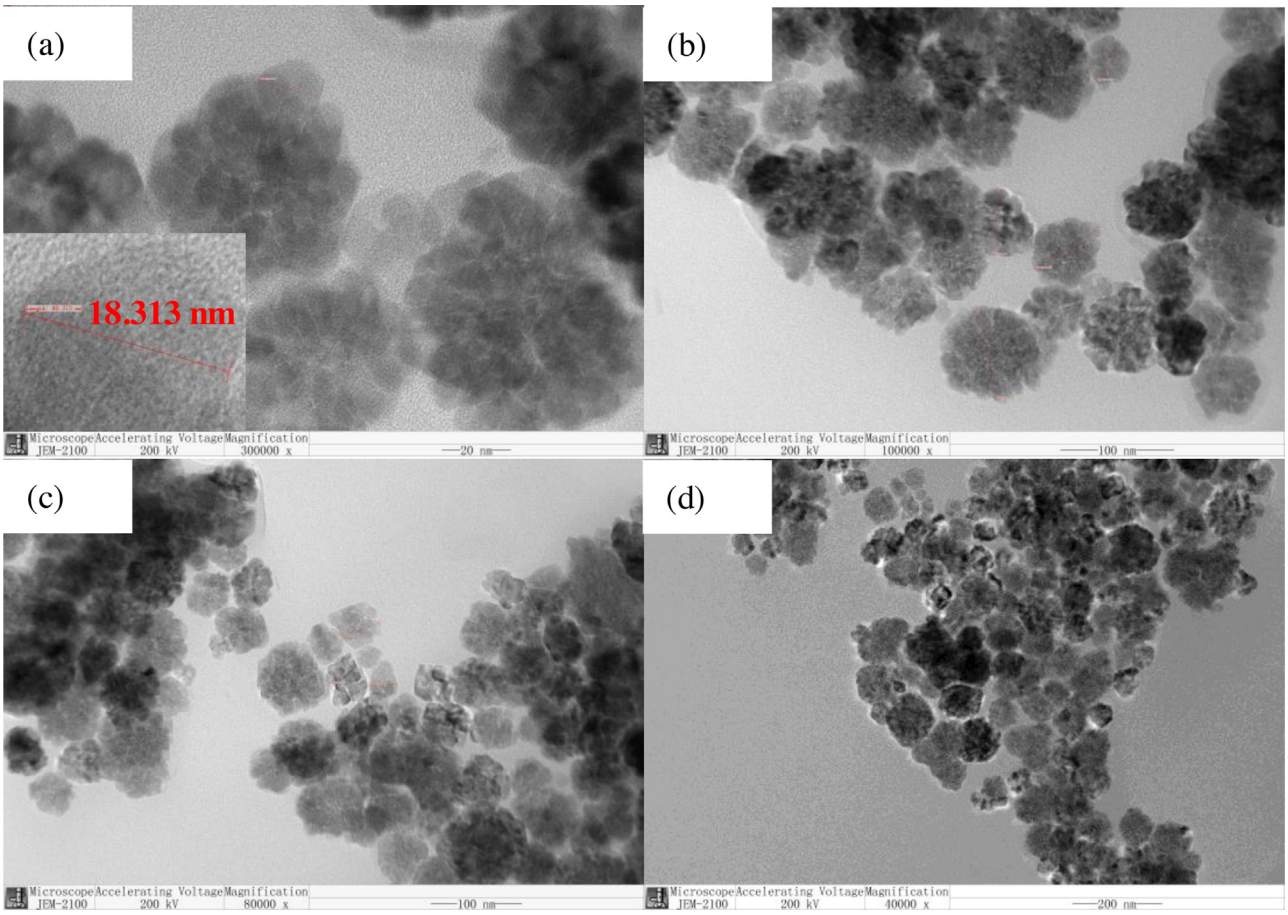

Fig. 3. Typical TEM images at high magnification (a) and low magnification (b–d) of fresh $ZnFe_2O_4$ powders.

Ltd., Guangdong, China), and the emission spectrum of the lamp (λ_{max} = 454 nm) was determined (Fig. S2, Supplementary data). The irradiation flux of visible light power was measured using a solar power meter (SM206, Shenzhen Sanpometer Ltd., China). During each experiment, a stock solution of 200 mL Orange II was placed in a 250 mL glass beaker and the initial concentration (C_0) was set at 100 mg/L. Unless otherwise specified, the initial pH (pH_0) of the dye solution was adjusted by using 0.1 mol/L sulfuric acid and 0.1 mol/L sodium hydroxide. The catalyst was added into the Orange II solution at the same time with constant stirring (around 500 rpm) by using a magnetic stirrer (C-MAG, HS7, IKA, Germany) for 30 min to reach absorption–desorption equilibrium in the dark conditions before the photocatalytic process was initiated. Subsequently, H_2O_2 was added and visible light irradiated on the suspension immediately. All the tests were performed at constant temperature (20 ± 2 °C) by using cooling bath. At given time intervals, 1.0 mL aliquots were filtered through the 0.22 μm membrane and immediately mixed with methanol (Orange II sample: methanol = 1:1 V/V) prior to analysis.

2.5. Analytical methods

The absorbance of samples was recorded at the wavelength of 485 nm on a Rayleigh UV-9100 spectrophotometer (Rayleigh Co., China). The removal efficiency of Orange II was obtained by Eq. (4), where C_0 and C were the concentration of Orange II sample at time 0 and t, respectively.

$$\text{Decolorization efficiency}(\%) = \frac{C_0 - C}{C_0} \times 100 \quad (4)$$

The concentration of H_2O_2 was detected based on a potassium titanium oxalate method [30]. Iron and zinc ions leaching concentrations were determined by an atomic absorption spectrophotometer (AAS, PerkinElmer A Analyst 800). The $^{\bullet}OH$ concentration was determined by the methyl sulfoxide trapping method to generate formaldehyde [31], which was then measured according to the Standard of People's Republic of China for Environment Protection (HJ 601-2007) [32]. Fluorometric measurements were conducted by F-4500 Fluorescence Spectrophotometer (Hitachi, Japan). UV–vis spectra were obtained using UV-1700 Spectrophotometer (Shimadzu, Japan).

GC–MS (VARIAN 450-GC/320-MS) analyses were applied to determine the intermediates [33,34] (Supplementary data). The TOC was detected by a Jena multi N/C 3100 (Supplementary data). COD was measured by a closed reflux spectrophotometric method according to the Standard of People's Republic of China for Environment Protection (HJ/T 399-3007) [35]. The toxicity of the solution was monitored with activated sludge similar to the work of Arslan-Alaton and co-workers [36,37] (see Supplementary data for detail). The percent of oxygen consumption inhibition (I_{OUR}, in %), for every treated sample was calculated using Eq. (5) [36,37], where OUR_S and OUR_B were the OUR value of samples in the reaction and in the blank, respectively.

$$I_{OUR}(\%) = \frac{[(OUR_B - OUR_S) \times 100]}{OUR_B} \quad (5)$$

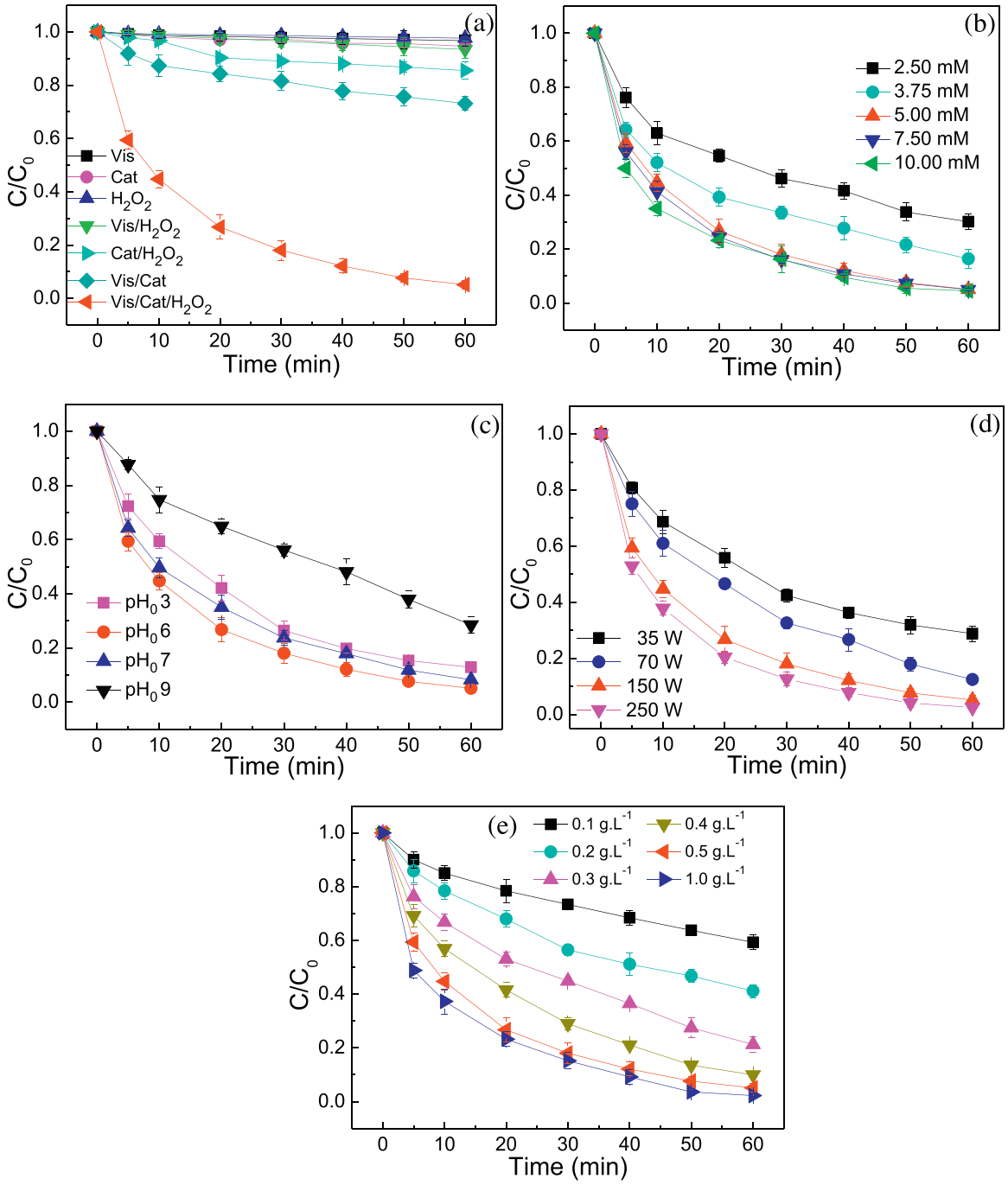

Fig. 4. (a) Decolorization of Orange II under different systems; effect of reaction parameters on the decolorization of Orange II: (b) effect of H_2O_2 concentration, (c) effect of pH_0, (d) effect of visible light power; (e) effect of catalyst dosage (C_0 = 100 mg/L, [H_2O_2] = 5.00 mM, [catalyst] = 0.5 g/L, P = 150 W, T = 20 ± 2 °C, pH_0 6) error bars represent the standard error of the mean for three replicates.

3. Results and discussion

3.1. Characterization of $ZnFe_2O_4$ catalysts

The crystalline nature and composition of the as-synthesized $ZnFe_2O_4$ catalyst and the corresponding samples after 5 cycles of photochemical reaction for degradation of Orange II were first characterized by XRD. As depicted in Fig. 1(a), the peaks at 2θ values of 78.4°, 73.5°, 70.5°, 62.2°, 56.6°, 53.1°, 42.8°, 36.8°, 35.2°, 29.9° and 18.2° could be ascribed to (4 4 4), (5 3 3), (6 2 0), (4 4 0), (5 1 1), (4 2 2), (4 0 0), (2 2 2), (3 1 1), (2 2 0) and (1 1 1) crystal planes of cubic $ZnFe_2O_4$ (JCPDS No. 82-1049), respectively [13,14]. The results confirmed that all diffraction peaks in Fig. 1(a) could be attributed to $ZnFe_2O_4$ with the cubic spinel structure (space group: Fd-3 m (2 2 7)). Moreover, the samples display broad diffraction lines, suggestive of small scattering domain sizes [26]. The domain size of coherent diffraction lies in the range of 15–30 nm, which was calculated from the data of full-width at half-maximum (FWHM) of the (4 4 0), (5 1 1), (4 0 0), (3 1 1), and (2 2 0) diffractions through the Scherrer equation. The diffraction patterns (Fig. 1(a)) of $ZnFe_2O_4$ catalyst after 5 cycles (used catalyst) of testing of photocatalytic activity were essentially similar to that of $ZnFe_2O_4$ before the photocatalytic testing, and no noticeable deviation was observed, indicative of high stability of $ZnFe_2O_4$ samples.

FTIR spectra of the $ZnFe_2O_4$ ferrite samples are shown in Fig. 1(b). The absorption broad band at 3420 cm^{-1} can be regarded as the stretching mode of H_2O molecules and OH groups, indicating the existence of H_2O molecules on the surface of the $ZnFe_2O_4$ nanoparticles [14,38]. The band at ~2360 cm^{-1} represents the absorbance of CO_2 from ambient air [39]. The band around ~1600 cm^{-1} (1610 cm^{-1}) corresponds to the bend style of H_2O molecules [38]. The observed band at around 1380 cm^{-1} can be indicative of the presence of nitrate. The band observed at ~564 cm^{-1} can be attributed to the tetrahedral Zn^{2+} (Zn—O mode) stretching vibration, and the band at ~436 cm^{-1} can be ascribed to the octahedral Fe^{3+} (Fe—O mode) stretching vibration [40]. In addition, almost no difference was discovered in the FTIR spectra of the $ZnFe_2O_4$ before and after 5 cycles of the Vis-Fenton reaction (Fig. 1(b)).

The porous nature of the $ZnFe_2O_4$ catalyst was investigated through nitrogen adsorption–desorption isotherm experiments to acquire further information on the properties relevant to the catalytic behavior of the catalyst. As displayed in Fig. 1(c), the isotherm is hithermost in shape to type IV. Such type clearly depicts the mesoporous nature of the $ZnFe_2O_4$ catalyst [19], and the hysteresis loop at high relative pressure (P/P_0) in the range of 0.50–1.00 shows that the mesopores are irregular in the catalyst [17]. Further investigation of the BJH pore size distribution confirmed the results. Fig. 1(d) shows a narrow peak centered at about 2.3 nm and the wider pore size in the range of 4.0–100.0 nm, which could be ascribed to the intraparticle pores within the $ZnFe_2O_4$ particles and the anomalous sizes and shapes of the pores from the aggregation of the $ZnFe_2O_4$ particles, respectively [17]. Similar isotherm and BJH pore size distribution results were observed for the used catalyst. Moreover, the BET specific surface area (46.5 m^2/g) of the used catalyst dropped insignificantly compared to the fresh catalyst (56.4 m^2/g), and the same trends were obtained for the pore volume and size of the samples (Table S1). All the results indicated the high stability of the $ZnFe_2O_4$ catalyst during the Vis-Fenton process.

FESEM images displayed the morphology of fresh and used $ZnFe_2O_4$ samples (Fig. 2). These images illustrate that fresh and used $ZnFe_2O_4$ samples exhibit a homogeneous arrangement of aggregated nanoparticles. In Fig. 2(a) and (c), the sphere-like nanoparticles with an average size of approximate 20–40 nm can be clearly observed, where this range of size is close to the value calculated by XRD analysis. The EDS results (see the inset in Fig. 2(b)) reveal that the atomic ratio of Zn/Fe/O of the $ZnFe_2O_4$ sample is approximate 1:2:4, which is in close proximity to the stoichiometric composition of $ZnFe_2O_4$ catalyst. In addition, comparison of the FESEM images of fresh and used $ZnFe_2O_4$ catalysts shows that there are no remarkable differences between the fresh and used $ZnFe_2O_4$ catalyst, indicating the catalyst is highly stable during the photocatalytic reactions.

The morphology of $ZnFe_2O_4$ powders are depicted by TEM in Fig. 3 exhibit uniform attachment of the $ZnFe_2O_4$ nanoparticles. It is interesting to notice that the $ZnFe_2O_4$ powders possess good spherical shape and this is consistent with the SEM results. The images also clearly demonstrate that the nanoparticle sizes range from about 15 to 30 nm, in good consistency with the sizes obtained from FWHM in XRD pattern using the Scherrer equation, indicating that $ZnFe_2O_4$ nanoparticles are monodisperse nanocrystals.

The optical absorption spectra of the $ZnFe_2O_4$ samples are illustrated in Fig. S3. The results demonstrate that the catalysts exhibit excellent Vis light absorption in the range of 450–700 nm for both the fresh and used catalyst, and this is crucial for Vis light catalytic reactions [19]. Moreover, the absorption with shoulder for the samples in the Vis region might result from the photoexicited electron transition from O 2p level into the Fe 3d level [17,19]. In addition, the absorption spectra of the $ZnFe_2O_4$ catalyst after 5 cycles of reaction are nearly the same as that of fresh catalyst (Fig. S3). The result also reveals that the $ZnFe_2O_4$ catalysts are of high stability under the Vis light catalytic reaction.

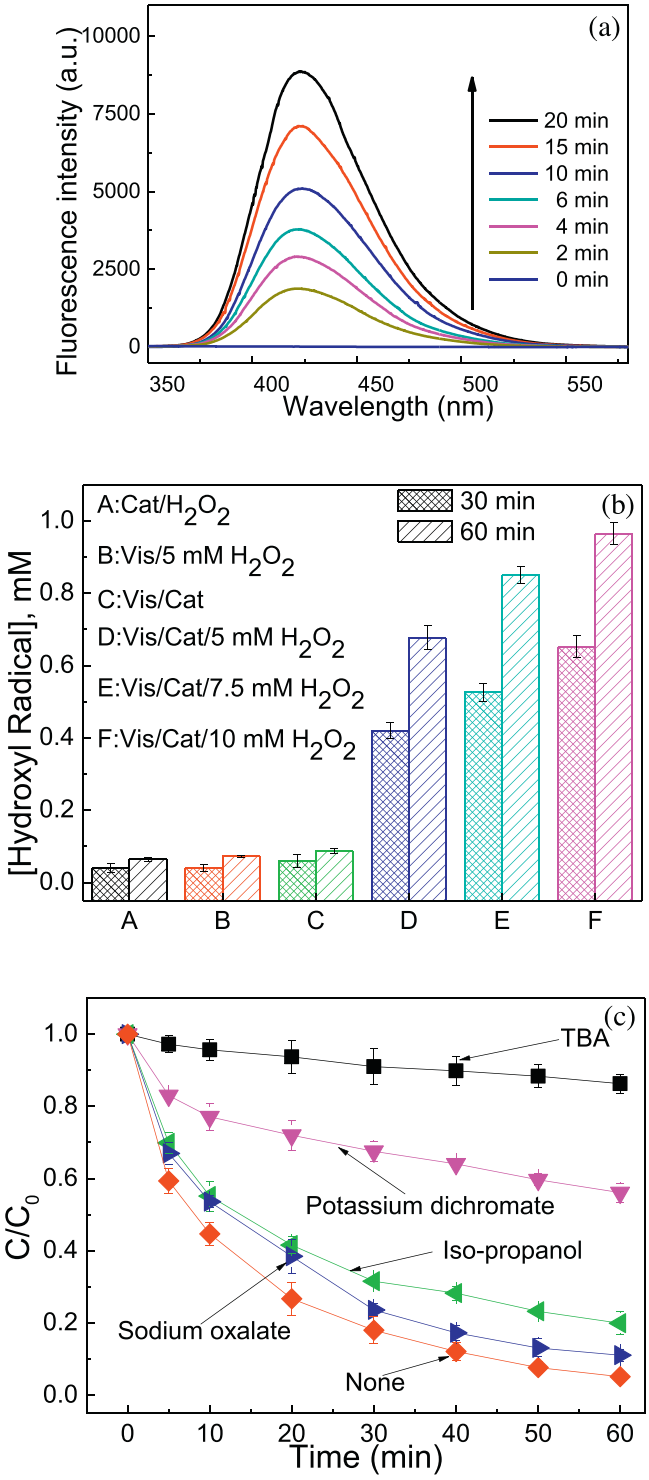

Fig. 5. (a) Fluorescence spectral changes of TAOH with irradiation time, (b) concentration of •OH generated at various reaction processes, (c) effect of radical scavengers on the decolorization of Orange II (C_0 = 100 mg/L, [Scavengers] = 0.1 M, [H_2O_2] = 5.00 mM, [catalyst] = 0.5 g/L, P = 150 W, T = 20 ± 2 °C, pH_0 6) error bars represent the standard error of the mean for three replicates.

Generally, the XRD, BET, SEM, and UV–vis DRS results demonstrate that the $ZnFe_2O_4$ particles remain nearly the same surface, bulk and structure during the reaction. Therefore, the $ZnFe_2O_4$

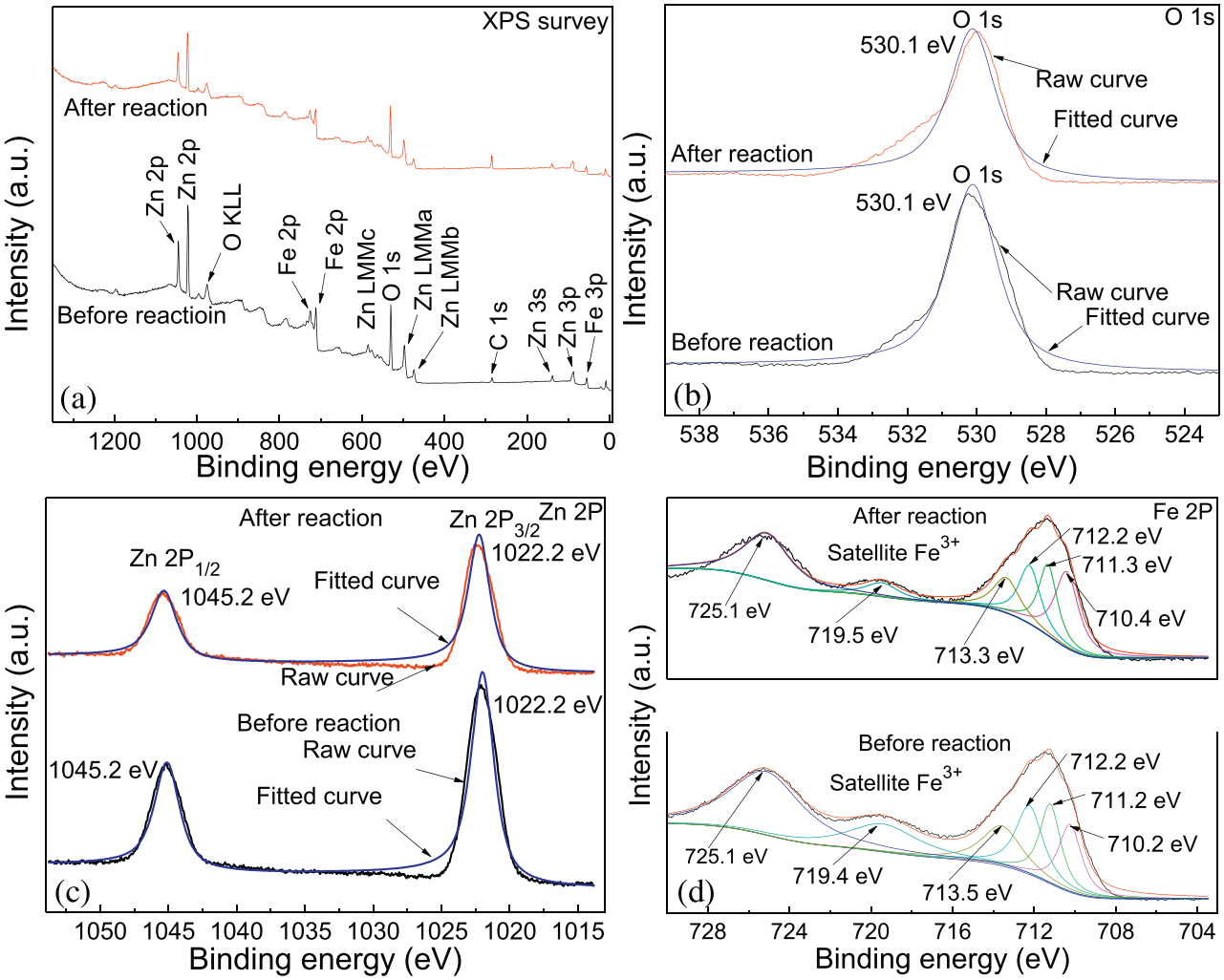

Fig. 6. The XPS spectra of whole XPS spectra (a) and typical elements O 1s (b), Zn 2p (c), Fe 2p (d).

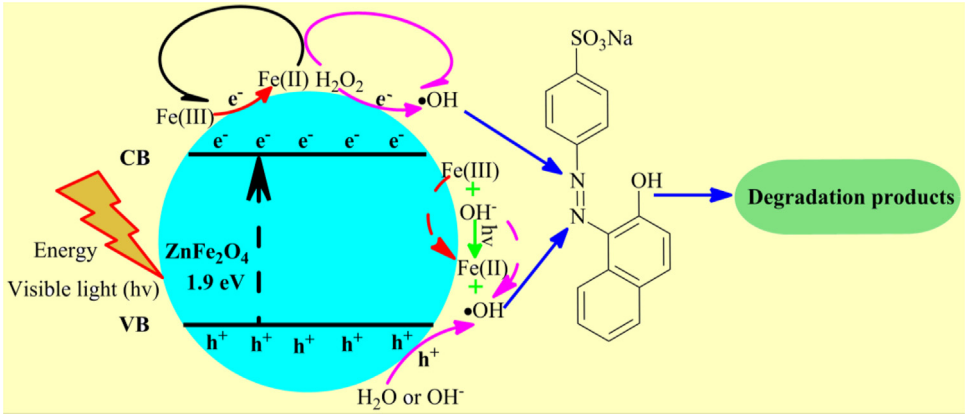

Fig. 7. Proposed mechanism of Vis/$ZnFe_2O_4$/H_2O_2 system.

catalyst can be applied as stable Vis light responsive catalyst for the treatment of aqueous contaminants.

3.2. Photocatalytic activity of $ZnFe_2O_4$

3.2.1. Degradation of Orange II under different systems

Fig. 4(a) shows the degradation efficiency under different experimental conditions. As shown in Fig. 4(a) and Table S1, negligible decolorization efficiency was obtained when Orange II was with H_2O_2 alone (2.3%) because of the limited oxidation power of H_2O_2 (E^0 = 1.76 V/SHE) [41], and 98.8% of H_2O_2 remaining after 60 min reaction, indicating that little H_2O_2 was decomposed in this situation. Only 3.7% and 6.6% of Orange II was removed by visible (Vis) light alone and Vis/H_2O_2, respectively. The decolorization efficiency was only 5.4% when the catalyst was applied alone, indicating that the influence of adsorption on Orange II was minimal

under the conditions. However, a slight increase was observed when the catalyst was combined with H_2O_2 (14.4%), and the H_2O_2 remaining was 86%, clearly demonstrating the possible role of the heterogeneous dark Fenton reaction as shown in Eq. (6) [19]. Moreover, a much higher efficiency (26.8%) was obtained under Vis/catalyst system. When with Vis light, the holes and electrons can be generated by the band gap radiation of the $ZnFe_2O_4$ particles (Eq. (7)) [26,27]. The holes in the VBM (valence band maximum) of the catalyst could remove Orange II by direct oxidation or formation of •OH via the reaction with the surface-adsorbed OH group (Eqs. (8) and (9)) [42]. Simultaneously, the superoxide radicals ($O_2^{\bullet-}$) might be formed via the capture of the electrons in the CBM (conduction band minimum) by O_2 [14,43]. Unfortunately, it is difficult for the photo-generated electron–holes to be effectively utilized due to their rapid recombination [43]. Therefore, the photocatalytic activity was relatively low in Vis/catalyst system.

The removal of Orange II was significantly enhanced with the simultaneous presence of $ZnFe_2O_4$ and H_2O_2 under Vis light irradiation. As illustrated in Fig. 4(a) and Table S2, the decolorization efficiency of Orange II increased significantly to 94.9% in Vis/$ZnFe_2O_4$/H_2O_2 system. The percentage of H_2O_2 remaining (21.6%) was the lowest in all of the processes involving H_2O_2. This can be explained by several aspects, according to the equations (Eqs. (6) and (12)) [44,45]. Apart from the small part of decolorization of Orange II by holes in this system (Eqs. (8) and (9)), electrons played an important role for removal of Orange II in Vis/$ZnFe_2O_4$/H_2O_2 system. In the presence of H_2O_2, electrons were more likely to be captured by H_2O_2 (E^0 (H_2O_2/•OH) = +0. 38 V vs. SCE) than by oxygen (E^0 ($O_2/O_2^{\bullet-}$) = −0. 33 V vs. SCE) to generate •OH (Eq. (10)) [19,27]. Simultaneously, H_2O_2 could be activated by the continuously regenerated Fe(II) (Eq. (6)), which could be formed from reaction of Fe(Ⅲ) with electrons (E^0 (Fe(III)/Fe(II)) = +0.77 V vs. SCE) (Eq. (11)). Thereby, the recombination of holes and electrons was apparently diminished and consequently more •OH could be generated for the degradation of Orange II [19]. The kinetics for the removal of Orange II followed the pseudo-first-order reaction (Table S2). The rate constant of the Vis/$ZnFe_2O_4$/H_2O_2 process was 0.0468 min^{-1}, while those of Vis, $ZnFe_2O_4$/H_2O_2 system were 0.0005 and 0.0027 min^{-1}, respectively. The results apparently indicated the synergistic effect between catalytic and photochemical decolorization of Orange II, especially clarifying the vital role of the visible light for the degradation of Orange II under $ZnFe_2O_4$/H_2O_2 system. Therefore, the quantum yield (Φ) was calculated to investigate the photocatalytic degradation efficiency and the value was $3.96 \pm 0.19 \times 10^{-3}$ (details in Supplementary data) [46,47].

$$H_2O_2 + Fe(II) \rightarrow Fe(III) + {}^{\bullet}OH + OH^- \quad (6)$$

$$ZnFe_2O_4 + h\nu \rightarrow ZnFe_2O_4(h^+ + e^-) \quad (7)$$

$$h^+ + H_2O \rightarrow H^+ + {}^{\bullet}OH \quad (8)$$

$$h^+ + OH^- \rightarrow {}^{\bullet}OH \quad (9)$$

$$H_2O_2 + e^- \rightarrow {}^{\bullet}OH + OH^- \quad (10)$$

$$Fe(III) + e^- \rightarrow Fe(II) \quad (11)$$

$$^{\bullet}OH + \text{Orange II} \rightarrow \text{degraded products} \quad (12)$$

3.3. Effect of reaction parameters on the decolorization of Orange II

3.3.1. Effect of the H_2O_2 concentration

Results of the study on the effect of initial H_2O_2 concentration (2.50, 3.75, 5.00, 7.50 and 10.00 mM) are provided in Fig. 4(b) and Table S2. When initial H_2O_2 concentration increased from 2.50 to 5.00 mM, the removal efficiency increased from 69.8% to 94.9% and the rate constant increased from 0.0182 to 0.0468 min^{-1}, respectively. However, when H_2O_2 concentration was increased further to 10 mM, a small difference was observed; the removal efficiency and rate constant increased only to 95.4% and 0.0487 min^{-1}, respectively. This may be ascribed to the unfavorable consumption of •OH by the excess H_2O_2, a reaction that scavenges •OH and generates $^{\bullet}HO_2$ in Eq. (13), the latter of which would also react with •OH (Eq. (14)) [48,49]. Moreover, the radical–radical reaction (Eq. (15)) may occur in competition to radical–organic reactions [50], thus leading to the more consumption of •OH, which would not be consumed by the dye. Therefore, the amount of H_2O_2 consumption increased from 2.03 to 6.48 mM with the increase of H_2O_2 concentration (Table S2). Based on the results, 5 mM of H_2O_2 was used in subsequent experiments.

$$^{\bullet}OH + H_2O_2 \rightarrow {}^{\bullet}HO_2 + H_2O \quad (13)$$

$$^{\bullet}HO_2 + {}^{\bullet}OH \rightarrow O_2 + H_2O \quad (14)$$

$$^{\bullet}OH + {}^{\bullet}OH \rightarrow H_2O_2 \quad (15)$$

3.3.2. Effect of initial pH (pH_0)

The influence of initial pH on the decolorization of Orange II was investigated at pH_0 3, 6, 7 and 9. It is easily observed from Fig. 4(c) that the decolorization efficiency of Orange II increased slightly with parallel increase in pH and exhibited the peak value at pH 6. However, subsequent increase of initial pH led to the decrease in decolorization of Orange II. When pH of Orange II varied from 3 to 6, the decolorization of Orange II increased slightly from 87.1% to 94.9%, and the rate constants increased from 0.0350 to 0.0468 min^{-1} while the percentage of remaining H_2O_2 decreased from 28.8% to 21.6% (Table S2). This may be due to the formation of different complexes on the catalyst hydration shell at different values of solution pH. When aqueous solutions became more acidic, the shell protonation of catalytic $Fe(H_2O)_6^{3+}$ would lead to the release of hydration shell water, thus influencing the reaction between catalytic species and H_2O_2 [13]. When the initial pH of Orange II was 7, the decolorization efficiency decreased slightly to 91.7%, the rate constant declined to 0.0389 min^{-1}, and the percentage of H_2O_2 remaining increased to 27.2%. However, when initial pH rose to 9, the color removal efficiency of Orange II decreased significantly to 71.5%, and the rate constant decreased to 0.0193 min^{-1}. This can be explained by the replacement of H_2O groups by OH^- groups at alkaline pH, and the adsorption of H_2O_2 on the catalyst would decrease as the catalyst was covered with of $Fe(OH)_6^-$, thus affecting the reaction between catalytic species and H_2O_2 [51]. Furthermore, the decomposition percentage of H_2O_2 was 73.2% at pH 9, which is expected since the decomposition of H_2O_2 into H_2O and O_2 in alkaline solution can be very fast [13].

The results reveal that both highly acidic and basic conditions are detrimental to the Vis/$ZnFe_2O_4$/H_2O_2 process to generate •OH, and the pH values around neutral and slightly acidic are beneficial for removal of Orange II. Therefore, the natural pH of Orange II (pH_0 6.0) was selected in subsequent experiments.

3.3.3. Effect of the visible light irradiation

The purpose of the experiments was to study the role of Vis light power for removal of Orange II. Various tests with Vis light powers at 35, 70, 150, and 250 W were performed. The experiments were performed at initial dye concentration of 100 mg/L, H_2O_2 concentration of 5.00 mM, $ZnFe_2O_4$ catalyst dose of 0.5 g/L, pH_0 6 and room temperature (20 ± 2 °C). As shown in Fig. 4(d) and Table S2, the decolorization of Orange II increased from 71.2% to 94.9%, the rate constant increased from 0.0205 to 0.0468 min^{-1}, and the percentage of H_2O_2 remaining decreased from 45.2% to 21.6% when Vis power was increased from 35 to 150 W. The results can be explained by several aspects. Generally, higher Vis power

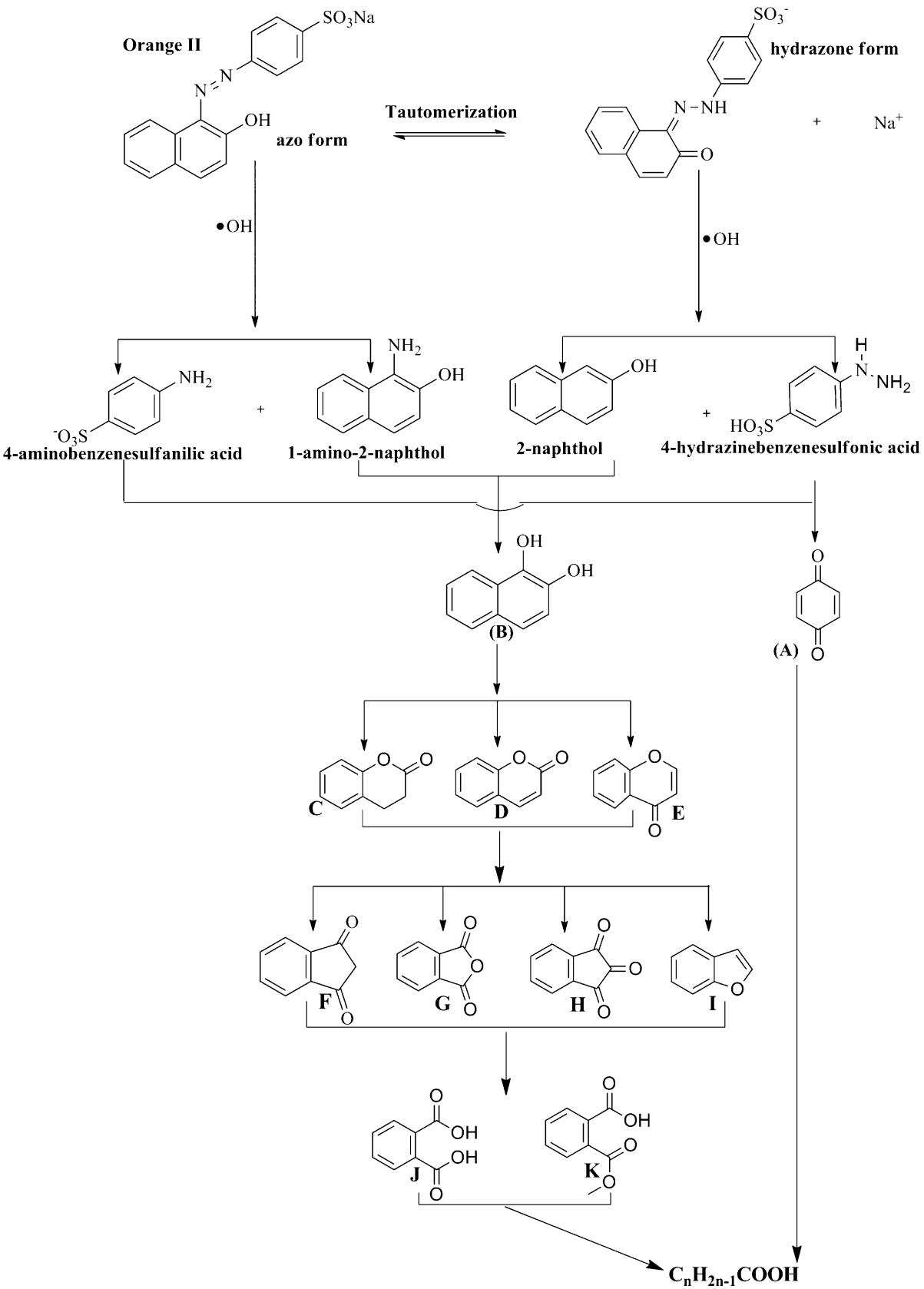

Fig. 8. Proposed pathways for degradation of Orange II (C_0 = 100 mg/L, [H_2O_2] = 5.00 mM, [catalyst] = 0.5 g/L, P = 150 W, T = 20 ± 2 °C, pH_0 6).

would make more Vis light photons absorbed by the $ZnFe_2O_4$ catalyst and accelerate the formation of electrons and holes on the surface of the catalyst, thus enhancing the decolorization of Orange II. With Vis light power further increasing to 250 W, the decolorization of Orange II increased to 97.6%, the rate constant elevated to 0.0584 min^{-1}, and the percentage of H_2O_2 remaining declined to 18.4%, respectively. However, considering the removal efficiency and energy consumption, 150 W of Vis power was selected in the following experiments.

3.3.4. Effect of the catalyst dosage

The experiments were performed to observe the decolorization of Orange II with different catalyst dosage in the range of 0.1–1.0 g/L. As depicted in Fig. 4(e) and Table S2, when the catalyst dosage increased from 0.1 to 0.5 g/L, the decolorization efficiency of Orange II increased from 40.7% to 94.9%, the rate constant increased from 0.0081 to 0.0468 min^{-1}, and the percentage of H_2O_2 remaining decreased from 68.4% to 21.6%. When higher dosage of $ZnFe_2O_4$ catalyst was applied, more electrons could be generated (Eq. (7)) and the regeneration of Fe(II) could be enhanced (Eq. (11)), eventually accelerating the decomposition of H_2O_2 to •OH. Overall, the increase in catalyst dosage would lead to more production of active sites in the system for reaction with oxidant to generate more reactive radicals, thus enhancing the decolorization of Orange II. However, when catalyst dosage further increased to 1.0 g/L, a slight improvement was observed, i.e., the decolorization efficiency of Orange II was 97.7%, the rate constant was 0.0587 min^{-1}, and the remaining percentage of H_2O_2 was 17.8%. When the $ZnFe_2O_4$ catalyst was over added, decomposition of H_2O_2 was increased and extra •OH would be formed, leading to the unfavorable reactions between radicals (Eqs. (14) and (15)). In addition, the •OH could be captured by the excess Fe(II) on the surface of the catalyst Eq. (16) [1]. Consequently, considerable •OH radicals were consumed without oxidizing Orange II. Therefore, 0.5 g/L of $ZnFe_2O_4$ was selected as the catalyst dosage for the following experiments.

$$\bullet OH + Fe(II) \rightarrow OH^- + Fe(III) \quad (16)$$

3.4. Possible mechanism

It is considered that •OH can be generated by Vis/$ZnFe_2O_4$/H_2O_2 process. To demonstrate this hypothesis, the fluorescent probe terephthalic acid (TA), which can easily react with •OH to generate highly fluorescent 2-hydroxy terephthalic acid (TAOH), was employed in the Vis/$ZnFe_2O_4$/H_2O_2 system [13,14]. Fig. 5(a) shows the changes of fluorescence spectra from the 1.0 mM TA and 5.00 mM H_2O_2 solution with irradiation time. It is interesting to see that the fluorescence intensity at around 425 nm increased significantly with the irradiation time, suggesting the formation of •OH [13,14]. These results indicate that •OH can be generated by Vis light irradiation in conjunction with $ZnFe_2O_4$ catalyst and H_2O_2.

Based on the fluorescent results, •OH concentrations were measured under various systems. As shown in Fig. 5(b), only a small amounts of •OH was generated in $ZnFe_2O_4$/H_2O_2, Vis/H_2O_2, and Vis/$ZnFe_2O_4$ system (Bars A–C). However, significant amounts of •OH were produced by the Vis/$ZnFe_2O_4$/H_2O_2 system (Bars D–F), owing to the catalytic decomposition of H_2O_2 and the oxidation of H_2O/OH^- by the photogenerated holes. In addition, the formation of •OH increased with the increase in H_2O_2 concentration (Bars D–F). The results reveal that large amounts of •OH can be generated under Vis/$ZnFe_2O_4$/H_2O_2 system and the yield of •OH was significantly enhanced compared with other systems.

To further elucidate the roles of •OH and other reactive species for the removal of Orange II in the Vis/$ZnFe_2O_4$/H_2O_2 system, experiments about radicals, holes and electrons trapping were also employed (Fig. 5(c)). The *tert*-butanol (TBA) and *iso*-propanol were applied as •OH radical scavengers to verify the role of •OH both in the solution and on the surface of the catalyst [52]. TBA has a rate constant with •OH in the range of 3.8–7.6 × 10^8 M^{-1} s^{-1} [53]. Generally, TBA is widely used as •OH scavenger both for heterogeneous and homogeneous systems, due to its ability to be easily adsorbed on the surface of the catalyst, which can occupy the reactive sites and finally inhibit the reaction process [52]. Therefore, TBA could be utilized as an effective capture agent for the •OH formed in water solution and on the surface of $ZnFe_2O_4$ catalyst. As depicted in Fig. 5(c), in the absence of radical scavenger, the decolorization rate constant and decolorization efficiency were 0.0468 min^{-1} and 94.9%, respectively. After 60 min reaction, the percentage of H_2O_2 remaining was 21.6% (Table S2). The oxidation process was suppressed significantly when TBA was applied into the reaction system. When 0.1 M TBA was added into the system, the decolorization rate declined to 0.0023 min^{-1} (Table S3) and led to a 81.2% drop in decolorization efficiency, indicating the vital part of •OH for the removal of Orange II. To investigate the function of $\bullet OH_{free}$ and $\bullet OH_{ads}$ on the decolorization of Orange II, *iso*-propanol, which has very low affinity to the surface of semiconductor in aqueous solution was employed as a well indicative of $\bullet OH_{free}$ [52,54]. The addition of 0.1 M *iso*-propanol inhibited the oxidation process with decolorization efficiency decreasing from 94.9% to 77.6% (i.e., reducing by 17.3%), indicating the effect of $\bullet OH_{free}$ produced in bulk solution was limited. These results suggest that the attack of $\bullet OH_{ads}$ generated on the surface of the catalyst was mainly responsible for the removal of Orange II. Comparatively, oxalate reacts weakly with •OH ($k = 4.7 \times 10^7$ M^{-1} s^{-1}), but it can be readily oxidized by h^+ [19,55]. As seen in Fig. 5(c), the degradation efficiency of Orange II with sodium oxalate (88.9%) was almost the same as that without scavenger (94.9%). The results also demonstrated that h^+ played an insignificant role in the oxidation reaction. Cr(VI) is normally employed as an efficient electron scavenger since the redox potential of Cr(VI) ($E^0(Cr_2O_7/Cr^{3+}) = +1.232$ V vs. SCE) is much higher than that of H_2O_2 (E^0 (H_2O_2/•OH) = +0.38 V vs. SCE) and Fe(III) (E^0 (Fe(III)/Fe(II)) = +0.77 V vs. SCE) [19,56,57]. As shown in Fig. 5(c), in the presence of 0.1 M Cr(VI), the decolorization of Orange II significantly decreased to 43.9% due to the preferential reaction between photogenerated electrons and Cr(VI), thus inhibiting the reactions of electrons with other species such as H_2O_2 and Fe(III). This result implies that photogenerated electrons are very important for the removal of Orange II.

On the basis of the discussion, the generation of reactive radicals and Orange II degradation primarily occurred on the catalyst surface. Therefore, further investigation of the elemental composition and chemical state of the $ZnFe_2O_4$ ferrite was performed by XPS analysis before and after the reaction. The survey XPS spectrum of the $ZnFe_2O_4$ ferrite confirms the predominant existence of Zn, Fe and O elements (Fig. 6(a)). The spectra were analyzed by XPSPEAK41 software and the curves are fitted well with the experimental results. In Fig. 6(b), the line shape of the core level O 1s was Gaussian-like with a binding energy of 530.1 eV, indicative of oxygen in the metal oxide. As depicted in Fig. 6(c), two distinct peaks at 1022.2 eV and 1045.2 eV could be attributed to the spectra of Zn $2p_{3/2}$ and Zn $2p_{1/2}$, respectively. There are no noticeable changes in the binding energies of the Zn 2p and O 1s peaks of $ZnFe_2O_4$ before and after the reaction. As shown in Fig. 6(d), the peaks at 725.1 eV and 719.2 eV are attributed to Fe $2p_{1/2}$ and shake-up satellite structure, respectively. For Fe $2p_{3/2}$ of the catalyst before reaction, four peaks at 710.2, 711.2, 712.2, and 713.5 eV were fitted for the spectrum [58,59]. The peak value of 710.2 eV can be ascribed to the existence of Fe(II) oxide, and the other three peaks can be attributed to the Fe(III) oxide [6]. It was calculated that the ratio between Fe(II) and Fe(III) on the surface of the catalyst elevated from 0.30 to 0.52 after the reaction, implying that Fe(II) was regenerated during the Vis/$ZnFe_2O_4$/H_2O_2 process.

According to the discussion above and previous reports [13,19,27], a probable photocatalytic mechanism for Vis/$ZnFe_2O_4$/H_2O_2 system is proposed in Fig. 7. When Vis light is used, charge separation in $ZnFe_2O_4$ particles occurs, and electrons are excited from the VB to the CB, leading to the simultaneous production of the holes in the VB (Eq. (7)) [13]. Then electrons can be effectively trapped by H_2O_2 to form •OH (Eq. (11)). Importantly, according to XPS analysis, Fe(II) can also be regenerated via the reaction between electrons and the surface Fe(III) (Eq. (10)). Simultaneously, Fe(II) can be obtained under Vis light irradiation of Fe(III) (Eq. (17)). Then more •OH can be produced as more Fe(II) is regenerated to react with H_2O_2 (Eq. (6)). Therefore, the degradation kinetics of the reaction between •OH and Orange II are greatly enhanced via visible light irradiation. Meanwhile, the holes can remove a small proportion of Orange II via Eqs. (8) and (9). Generally, the degradation of Orange II was primarily dominated due to the •OH formed from Reactions (6), (11), and (17).

$$Fe(III) + h\nu + OH^- \rightarrow Fe(II) + {}^{\bullet}OH \quad (17)$$

3.5. The degradation pathway of Orange II

In this study, UV–vis spectroscopy was used to analyze the samples (Fig. S4). It can be observed that the absorption spectrum of the untreated Orange II contains three major bands. One located at 485 nm is the main band associated to the azo bond. Additionally, the other two bands at 229 nm and 310 nm are associated to the benzene and naphthalene structures in the compound [34,60,61]. As displayed in Fig. S4, the absorption at visible band gradually decreased when the reaction proceeded, indicating the fragmentation of the azo bond. The reduction of absorbance at 229 nm together with 310 nm was indicative of aromatic ring breakage during the reaction [61].

Furthermore, the main intermediate products of Orange II were identified by GC–MS technique (Table S4). According to the results and previous studies [5,19,50,61], a possible pathway for Orange II degradation in the Vis/$ZnFe_2O_4$/H_2O_2 system is proposed in Fig. 8.

Generally, •OH attacks organic compounds by electron transfer, electrophilic addition, or hydrogen abstraction mechanism [5,62–64]. It is widely accepted that •OH is more likely to react with organics via electrophilic addition, or hydrogen abstraction reaction [63,65,66]. The 1-amino-2-naphthol and 4-aminobenzenesulfonic acid are generated by the electrophilic addition of •OH on N=N of Orange II [50,67,68]. Analogously, •OH attacks the hydrozone form of Orange II on C=N, leading to the production of 4-hydrazinebenzenesulfonic acid and 2-naphthol [65,67,68]. The sulfonic group makes 4-aminobenzenesulfonic acid and 4-hydrazinebenzenesulfonic acid molecules to have thermal stability and high solubility in aqueous solution. However, 2-naphthol and 1-amino-2-naphthol are sensitive to oxygen and can easily be oxidized under aerobic circumstances [69]. Therefore, none of these four products was detected in this study. The electrophilic attack of 2-naphthol or 1-amino-2-naphthol by •OH generates 1,2-naphthalenediol (B) [65,67]. Similarly, the further degradation of 4-aminobenzenesulfonic acid and 4-hydrazinebenzenesulfonic acid by •OH leads to the formation of benzoquinone (A) [1,7,50]. Meanwhile, 1,2-naphthalenediol is subsequently oxidized by •OH via electrophilic addition, to form alpha-tetralone (C), 2H-1-benzopyran-2-one (D), and 4H-1-benzopyran-4-one (E) [5,53,69]. These compounds are then further degraded to form five-atom ring heterocyclic compounds, such as 1,3-indanedione (F), indan-1,2,3-trione (G), phthalic anhydride (H), and benzofuran (I) [1,5,33,34,61,69]. The five-atom ring compounds can be broken down by the attack of •OH, giving rise to phthalic acid (J) and 1,2-benzenedicarboxylic acid, 1-methyl ester (K), both are benzene structure intermediate products [50,69]. Finally, these intermediate products are degraded to smaller molecules.

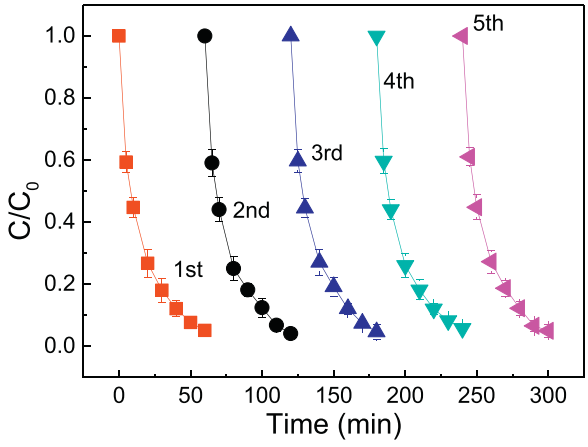

Fig. 9. Recycling study of the decolorization of Orange II (C_0 = 100 mg/L, [H_2O_2] = 5.00 mM, [catalyst] = 0.5 g/L, P = 150 W, T = 20 ± 2 °C, pH_0 6) error bars represent the standard error of the mean for three replicates.

3.6. Stability of $ZnFe_2O_4$ in multiple runs

Recycle tests were conducted to investigate the stability of $ZnFe_2O_4$ particles in the oxidation process under Vis light irradiation. The catalyst was easily separated, washed, dried in a vacuum oven and finally kept at room temperature. As shown in Fig. 9 and Table S5, in the first cycle, the decolorization efficiency was 94.9% after 60 min reaction, the reaction rate constant was 0.0468 min^{-1}, and the leaching zinc and iron concentrations were 0.0295 mg/L (leaching percent 0.022%) and 0.0541 mg/L (leaching percent 0.023%), respectively. The decolorization efficiency was 95.1% and the reaction rate constant achieved was 0.0483 min^{-1} in the fifth cycle and the leaching concentrations of zinc and iron decreased slightly to 0.0264 mg/L (leaching percent 0.019%) and 0.0482 mg/L (leaching percent 0.021%), respectively, implying that the catalyst is quite stable and could be reutilized. The percentage of H_2O_2 remaining was 21.6%, 20.4%, 20.8%, 22.4%, and 21.2%, respectively from the first to the fifth cycles. The results also revealed that the catalyst could decompose almost the same amount of H_2O_2 during the five successive cycles, indicative of high stability of the catalyst.

3.7. Mineralization and toxicity with reaction time

The changes of TOC and COD removal efficiency and the toxicity on activated sludge were performed with initial dye concentration of 100 mg/L, H_2O_2 concentration of 5.0 mM, catalyst dosage of 0.5 g/L, Vis power of 150 W, reaction temperature of 20 ± 2 °C and pH_0 6. The COD and TOC degradation depicted in Fig. 10 is clear evidence that the COD and TOC removal efficiencies of Orange II within 30 min of reaction were 55.4% and 35.7%, respectively, and these increased to 86.6% and 60.4% when time extended to 60 min. The toxicity of Orange II was studied by separate activated sludge inhibition experiments (see details in Supplementary data). From Fig. 10 it can be seen that the I_{OUR} value of the original Orange II was 14.6%, and the acute toxicity increased as the reaction proceeded. The rise of toxicity during the Vis/$ZnFe_2O_4$/H_2O_2 process suggests the appearance of more toxic intermediates. Fortunately, after 45 min reaction, the I_{OUR} value was only 5.2%, and the inhibitory value was nearly zero (0.07%) when the reaction time reached 60 min. The results demonstrated that the toxicity of the

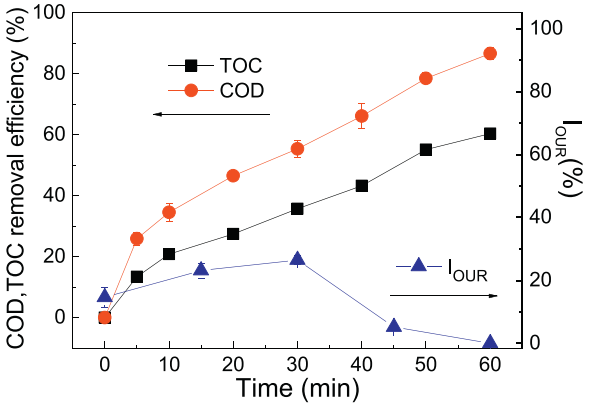

Fig. 10. The changes of COD, TOC and toxicity with reaction (C_0 = 100 mg/L, [H_2O_2] = 5.00 mM, [catalyst] = 0.5 g/L, P = 150 W, T = 20 ± 2 °C, pH_0 6) Error bars represent the standard error of the mean for three replicates.

Orange II and the degradation intermediates can be eliminated by the Vis/$ZnFe_2O_4$/H_2O_2 process.

4. Conclusions

The $ZnFe_2O_4$ photocatalyst was successfully synthesized by a two-step method. The catalyst displayed high photocatalytic activity for splitting H_2O_2 and for the removal of Orange II under irradiation by Vis light ($\lambda > 420$ nm). Orange II could be quickly degraded in a wide pH_0 range (3–7) because of the apparent production of sufficient •OH in this system. The catalyst exhibited good activity and stability under Vis irradiation. The decolorization efficiency was still over 94% after five reuse cycles and extremely low leaching of zinc and iron were observed. The study confirmed that •OH on the surface of the catalyst was the dominating oxidizing species in this process. The main intermediate products were determined and a possible degradation pathway of Orange II was proposed. The I_{OUR} experiment indicated that the toxicity of Orange II together with its degradation products could be eliminated. We believe that the $ZnFe_2O_4$ will be a promising catalyst for the photocatalytic treatment of dyes and other refractory wastewater organic pollutants in the presence of H_2O_2 and Vis irradiation.

Acknowledgement

This work was supported by Natural Science Foundation of Hubei Province, China (Grant No. 2012FFA089). The analysis of XPS, XRD, SEM, EDS, AAS, and GC–MS was partially supported by Large-scale Instrument and Equipment Sharing Foundation of Wuhan University. D.D. Dionysiou also acknowledges support from the University of Cincinnati through a UNESCO co-Chair Professor position on "Water Access and Sustainability".

Appendix A. Supplementary data

Supplementary data associated with this article can be found, in the online version, at http://dx.doi.org/10.1016/j.apcatb.2015.09.056.

References

[1] H. Lin, H. Zhang, X. Wang, L.G. Wang, J. Wu, Sep. Purif. Technol. 122 (2014) 533–540.
[2] M. Dükkancı, M. Vinatoru, T.J. Mason, Ultrason. Sonochem. 21 (2014) 846–853.
[3] M.L. Rache, A.R. García, H.R. Zea, A.M.T. Silva, L.M. Madeira, J.H. Ramírez, Appl. Catal. B: Environ. 146 (2014) 192–200.
[4] C. Cai, L.G. Wang, H. Gao, L.W. Hou, H. Zhang, J. Environ. Sci. China 26 (2014) 1267–1273.
[5] C. Cai, H. Zhang, X. Zhong, L.W. Hou, Water Res. 66 (2014) 473–485.
[6] H. Lin, H. Zhang, L.W. Hou, J. Hazard. Mater. 276C (2014) 182–191.
[7] H.Y. Li, Y.H. Gong, Q.Q. Huang, H. Zhang, Ind. Eng. Chem. Res. 52 (2013) 15560–15567.
[8] M. Wang, X. Liu, B. Pan, S. Zhang, Chemosphere 93 (2013) 2877–2882.
[9] M. Minella, G. Marchetti, E. De Laurentiis, M. Malandrino, V. Maurino, C. Minero, D. Vione, K. Hanna, Appl. Catal. B: Environ. 154–155 (2014) 102–109.
[10] H. Zhang, C. Fei, D.B. Zhang, F. Tang, J. Hazard. Mater. 145 (2007) 227–232.
[11] D. Rubio, E. Nebot, J.F. Casanueva, C. Pulgarin, Water Res. 47 (2013) 6367–6379.
[12] J. Herney-Ramirez, M.A. Vicente, L.M. Madeira, Appl. Catal. B: Environ. 98 (2010) 10–26.
[13] D.B. Lu, Y. Zhang, S.X. Lin, L.T. Wang, C.M. Wang, J. Alloys Compd. 579 (2013) 336–342.
[14] Y. Hou, X.Y. Li, Q.D. Zhao, G.H. Chen, Appl. Catal. B: Environ. 142–143 (2013) 80–88.
[15] M.B. Kasiri, H. Aleboyeh, A. Aleboyeh, Appl. Catal. B: Environ. 84 (2008) 9–15.
[16] N. Banić, B. Abramović, J. Krstić, D. Šojić, D. Lončarević, Z. Cherkezova-Zheleva, V. Guzsvány, Appl. Catal. B: Environ. 107 (2011) 363–371.
[17] H. Lv, L. Ma, P. Zeng, D. Ke, T. Peng, J. Mater. Chem. 20 (2010) 3665–3672.
[18] Y. Liu, Y. Zhu, J. Xu, X. Bai, R. Zong, Y.F. Zhu, Appl. Catal. B: Environ. 142–143 (2013) 561–567.
[19] M. Su, C. He, V.K. Sharma, M. Abou Asi, D. Xia, X.Z. Li, H. Deng, Y. Xiong, J. Hazard. Mater. 211–212 (2012) 95–103.
[20] L.D. Sánchez, S.F.M. Taxt-Lamolle, E.O. Hole, A. Krivokapić, E. Sagstuen, H.J. Haugen, Appl. Catal. B: Environ. 142–143 (2013) 662–667.
[21] C. Ruales-Lonfat, J.F. Barona, A. Sienkiewicz, M. Bensimon, J. Vélez-Colmenares, N. Benítez, C. Pulgarín, Appl. Catal. B: Environ. 166–167 (2015) 497–508.
[22] X. Li, Y. Hou, Q. Zhao, W. Teng, X. Hu, G. Chen, Chemosphere 82 (2011) 581–586.
[23] L. Su, J. Feng, X. Zhou, C. Ren, H. Li, X. Chen, Anal. Chem. 84 (2012) 5753–5758.
[24] J. Yang, X. Li, X. Deng, Z. Huang, Y. Zhang, J. Ceram. Soc. Jpn. 12 (2012) 579–583.
[25] G.L. Fan, Z.J. Gu, L. Yang, F. Li, Chem. Eng. J. 155 (2009) 534–541.
[26] G.L. Fan, J. Tong, F. Li, Ind. Eng. Chem. Res. 51 (2012) 13639–13647.
[27] Y.S. Fu, X. Wang, Ind. Eng. Chem. Res. 50 (2011) 7210–7218.
[28] S.J. Yuan, X.H. Dai, Appl. Catal. B: Environ. 154–155 (2014) 252–258.
[29] L. Lu, Z. Ai, J. Li, Z. Zheng, Q. Li, L. Zhang, Cryst. Growth Des. 7 (2007) 459–464.
[30] R.M. Sellers, Analyst 105 (1980) 950–954.
[31] C. Tai, J.F. Peng, J.F. Liu, G.B. Jiang, H. Zou, Anal. Chim. Acta 527 (2004) 73–80.
[32] Standard of the People's Republic of China for Environmental Protection, HJ 601–2011, 2011.
[33] C. Cai, H. Zhang, X. Zhong, L.W. Hou, J. Hazard. Mater. 283C (2015) 70–79.
[34] J. Wu, H. Zhang, J.J. Qiu, J. Hazard. Mater. 215–216 (2012) 138–145.
[35] Standard of the People's Republic of China for Environmental Protection, HJ-T 399–2007, 2007.
[36] I. Arslan-Alaton, N. Ayten, T. Olmez-Hanci, Appl. Catal. B: Environ. 96 (2010) 208–217.
[37] T. Olmez-Hanci, C. Imren, I. Arslan-Alaton, I. Kabdasli, O. Tunay, Photochem. Photobiol. Sci. 8 (2009) 620–627.
[38] P. Laokul, V. Amornkitbamrung, S. Seraphin, S. Maensiri, Curr. Appl. Phys. 11 (2011) 101–108.
[39] R. Rameshbabu, R. Ramesh, S. Kanagesan, A. Karthigeyan, S. Ponnusamy, J. Sol–Gel Sci. Technol. 71 (2014) 147–151.
[40] A. Meidanchi, O. Akhavan, Carbon 69 (2014) 230–238.
[41] X. Chen, W. Wang, H. Xiao, C. Hong, F. Zhu, Y. Yao, Z. Xue, Chem. Eng. J. 193–194 (2012) 290–295.
[42] W.Q. Zhang, M. Wang, W.J. Zhao, B.Q. Wang, Dalton Trans. 42 (2013) 15464–15474.
[43] X. Guo, H. Zhu, Q. Li, Appl. Catal. B: Environ. 160–161 (2014) 408–414.
[44] A. Rastogi, S.R. Ai-Abed, D.D. Dionysiou, Appl. Catal. B: Environ. 85 (2009) 171–179.
[45] P. Shukla, H.Q. Sun, S.B. Wang, H.M. Ang, M.O. Tade, Catal. Today 175 (2011) 380–385.
[46] J. Xu, J.J. Li, F. Wu, Y. Zhang, Environ. Sci. Technol. 48 (2014) 272–278.
[47] Y.W. Gao, Y. Wang, H. Zhang, Appl. Catal. B: Environ. 178 (2015) 29–36.
[48] Y.B. Wang, H.Y. Zhao, G.H. Zhao, Appl. Catal. B: Environ. 164 (2015) 396–406.
[49] X. Zhong, J. Barbier, D. Duprez, H. Zhang, S. Royer, Appl. Catal. B: Environ. 121–122 (2012) 123–134.
[50] X. Zhong, S. Royer, H. Zhang, Q.Q. Huang, L.J. Xiang, S. Valange, J. Barrault, Sep. Purif. Technol. 80 (2011) 163–171.
[51] J. Zhang, J. Zhuang, L. Gao, Y. Zhang, N. Gu, J. Feng, D. Yang, J. Zhu, X. Yan, Chemosphere 73 (2008) 1524–1528.
[52] L.W. Hou, H. Zhang, L.G. Wang, L. Chen, Chem. Eng. J. 229 (2013) 577–584.
[53] M.E. Lindsey, M.A. Tarr, Environ. Sci. Technol. 34 (2000) 444–449.
[54] L.S. Zhang, K.H. Wong, D.Q. Zhang, C. Hu, J.C. Yu, C.Y. Chan, P.K. Wong, Environ. Sci. Technol. 43 (2009) 7883–7888.
[55] Y. Mao, C. Schoeneich, K.D. Asmus, J. Phys. Chem. 95 (1991) 10080–10089.
[56] L.S. Zhang, K.H. Wong, H.Y. Yip, C. Hu, J.C. Yu, C.Y. Chan, P.K. Wong, Environ. Sci. Technol. 44 (2010) 1392–1398.
[57] J. Deng, Y. Shao, N. Gao, C. Tan, S. Zhou, X. Hu, J. Hazard. Mater. 262 (2013) 836–844.
[58] H.Y. Zhao, Y.J. Wang, Y.B. Wang, T.C. Cao, G.H. Zhao, Appl. Catal. B: Environ. 125 (2012) 120–127.
[59] L.Q. Guo, F. Chen, X.Q. Fan, W.D. Cai, J.L. Zhang, Appl. Catal. B: Environ. 96 (2010) 162–168.

[60] H. Zhang, H. Fu, D.B. Zhang, J. Hazard. Mater. 172 (2009) 654–660.
[61] H.Y. Li, Y.L. Li, L.J. Xiang, Q.Q. Huang, J.J. Qiu, H. Zhang, M.V. Sivaiah, F. Baron, J. Barrault, S. Petit, S. Valange, J. Hazard. Mater. 287 (2015) 32–41.
[62] G.P. Anipsitakis, D.D. Dionysiou, M.A. Gonzalez, Environ. Sci. Technol. 40 (2006) 1000–1007.
[63] A. Özcan, M.A. Oturan, N. Oturan, Y. Şahin, J. Hazard. Mater. 163 (2009) 1213–1220.
[64] A.H. Long, Y. Lei, H. Zhang, Ind. Eng. Chem. Res. 53 (2014) 1033–1039.
[65] I.K. Konstantinou, T.A. Albanis, Appl. Catal. B: Environ. 49 (2004) 1–14.
[66] A.S. Özen, V. Aviyente, G. Tezcanli-Güyer, N.H. Ince, J. Phys. Chem. A 109 (2005) 3506–3516.
[67] S. Hammami, N. Bellakhal, N. Oturan, M.A. Oturan, M. Dachraoui, Chemosphere 73 (2008) 678–684.
[68] A.S. Özen, V. Aviyente, R.A. Klein, J. Phys. Chem. A 107 (2003) 4898–4907.
[69] H.Z. Zhao, Y. Sun, L.N. Xu, J.R. Ni, Chemosphere 78 (2010) 46–51.